AI–AEC–12670

COPY

HELIUM EMBRITTLEMENT OF TYPE 316 STAINLESS STEEL

AEC Research and Development Report

AMPTIAC

DISTRIBUTION STATEMENT A:
Approved for Public Release -
Distribution Unlimited

ATOMICS INTERNATIONAL

A DIVISION OF NORTH AMERICAN ROCKWELL CORPORATION

Printed in the United States of America
Available from
Clearinghouse for Federal Scientific and Technical Information
National Bureau of Standards, U.S. Department of Commerce
Springfield, Virginia 22151
Price: Printed Copy $3.00; Microfiche $0.65

AI-AEC-12670
METALS, CERAMICS,
AND MATERIALS

HELIUM EMBRITTLEMENT OF TYPE 316 STAINLESS STEEL

By
D. KRAMER
K. R. GARR
C. G. RHODES*
A. G. PARD

*North American Rockwell Science Center, Thousand Oaks, California

ATOMICS INTERNATIONAL
A DIVISION OF NORTH AMERICAN ROCKWELL CORPORATION

CONTRACT: AT(04-3)-701
ISSUED: APRIL 30, 1968

DISTRIBUTION

This report has been distributed according to the category "Metals, Ceramics, and Materials" as given in the Standard Distribution for Unclassified Scientific and Technical Reports, TID-4500.

ACKNOWLEDGMENT

The authors are pleased to acknowledge the assistance of R. M. Kniefel with the tensile testing and cyclotron irradiations, and the contributions of R. A. Spurling and D. R. Warner to the metallography. This work was supported by the United States Atomic Energy Commission.

CONTENTS

	Page
Abstract	5
I. Introduction	7
II. Experimental	7
III. Results	9
A. Initial Microstructures	9
B. Tensile Test Results	9
C. Metallography of Tested Samples	15
IV. Discussion	28
V. Conclusions	30
References	31

TABLES

1. Tensile Test Data of Type 316 Stainless Steel With Treatment 6	14
2. Tensile Test Data of Type 316 Stainless Steel With Treatment 13	14

FIGURES

1. Replica Electron Micrograph of Type 316 Stainless Steel After Treatment 6, Showing Carbides Primarily on Grain Boundaries	10
2. Replica Electron Micrograph of Type 316 Stainless Steel After Treatment 13, Showing Precipitates on Grain Boundaries and Within the Grains	11
3. Transmission Electron Micrograph of Type 316 Stainless Steel After Treatment 13, Showing Sigma Particles Within a Grain	12
4. Total Elongation as a Function of Test Temperature for Type 316 Stainless Steel With no Helium and With 4×10^{-5} Atom Fraction Helium	13
5. Fractograph of Type 316 Stainless Steel Without Helium Tested at 540°C, Showing Shear-Rupture Dimples	16

FIGURES

Page

6. Light Micrographs of Type 316 Stainless Steel With 4×10^{-5} Atom Fraction Helium Tested at 760°C, Showing Intergranular Cracks 17

7a. Replica Electron Micrograph of Type 316 Stainless Steel With 4×10^{-5} Atom Fraction Helium Tested at 760°C, Showing Voids Adjacent to Grain-Boundary Carbides, Treatment 6 18

7b. Replica Electron Micrograph of Type 316 Stainless Steel With 4×10^{-5} Atom Fraction Helium Tested at 760°C, Showing Voids Adjacent to Grain-Boundary Carbides, Treatment 13. 19

8a. Transmission Electron Micrograph Showing Helium Bubbles in Type 316 Stainless Steel Given Treatment 6 With 4×10^{-5} Atom Fraction Helium Tested at 760°C 20

8b. Transmission Electron Micrograph Showing Helium Bubbles in Type 316 Stainless Steel Given Treatment 6 With 4×10^{-5} Atom Fraction Helium Tested at 760°C 21

8c. Transmission Electron Micrograph Showing Helium Bubbles in Type 316 Stainless Steel Given Treatment 6 With 4×10^{-5} Atom Fraction Helium Tested at 760°C 22

9a. Transmission Electron Micrograph Showing Helium Bubbles in Type 316 Stainless Steel Given Treatment 13 With 4×10^{-5} Atom Fraction Helium Tested at 760°C 24

9b. Transmission Electron Micrograph Showing Helium Bubbles in Type 316 Stainless Steel Given Treatment 13 With 4×10^{-5} Atom Fraction Helium Tested at 760°C 25

10a. Transmission Electron Micrograph Showing Fractured Carbide Particles in Type 316 Stainless Steel Given Treatment 6 With 4×10^{-5} Atom Fraction Helium, Tested at 540°C. 26

10b. Transmission Electron Micrograph Showing Fractured Carbide Particles in Type 316 Stainless Steel Given Treatment 6 With 4×10^{-5} Atom Fraction Helium, Tested at 650°C. 27

ABSTRACT

Helium was injected into small tensile samples of Type 316 stainless steel by alpha-particle irradiation from a cyclotron. Subsequent tensile testing in the temperature range 540 to 815°C revealed a loss of ductility, as measured by elongation at failure. The lowest temperature at which a ductility loss was manifest depended upon the microstructure of the samples. A fine dispersion of sigma particles within the matrix was capable of raising this temperature by retarding the accumulation of helium at grain boundaries.

Reduced ductility was always accompanied by partial or complete intergranular failure and the presence of intergranular cracks. These cracks originated as small voids adjacent to grain-boundary carbide particles, presumably through the action of grain-boundary sliding. Large helium bubbles found attached to carbide particles are responsible for the relative ease of void formation, as compared to samples without helium.

→ p 13

I. INTRODUCTION

The behavior of helium in stainless steel has been the subject of several investigations of mechanisms of bubble formation and embrittlement.[1-3]* The problem of He embrittlement is of great importance to fuel-cladding alloys in nuclear reactors. In a fast breeder reactor all the major constituents (iron, nickel, and chromium) of an austenitic cladding alloy transmute to other isotopes by (n,α) and (n,p) reactions yielding He and hydrogen.[4]

Embrittlement is identified as a loss in ductility at elevated temperatures and can be brought about with as little as 10^{-6} atom fraction He. This is due to its insolubility in steel and the tendency of He bubbles to concentrate at grain boundaries. Helium embrittlement in Type 304 stainless steel has recently been studied in detail with samples in which the He was introduced by α-particles from a cyclotron.[5] This approach is extended to Type 316 stainless steel in the work reported here.

II. EXPERIMENTAL

The technique of cyclotron injection of helium into small tensile samples has been reported elsewhere.[5] The samples have a gauge length of 0.50 in. and a cross-section of 0.009 in. x 0.040 in. During cyclotron injection the temperature of the samples is kept below 150°C. The He concentration, based on the total volume of the gauge portion of the sample, was determined by mass spectrometry to be $4 \pm 0.3 \times 10^{-5}$ atom fraction. However, the He is distributed uniformly only through the central two-thirds of the thickness. This distribution was achieved by variable attenuation of the α beam.

The composition in wt % of the Type 316 stainless steel used was: chromium 17.3, nickel 13.6, molybdenum 2.3, carbon 0.06, nitrogen 0.05, and the balance iron. Before injection of He the samples were given one of the two following treatments:

No. 6: 50% cold rolled, annealed 1 hr at 980°C and for 8 hr at 760°C.

*Superscript numbers in parentheses are for References at back of this report.

No. 13: Annealed 30 min at 1120°C, 25% cold rolled, annealed 24 hr at 480°C and for 144 hr at 705°C.

Between anneals they were cooled in vacuum.

The tensile tests were performed in vacuum and samples were held at test temperature for 1 hr before the load was applied.

III. RESULTS

A. INITIAL MICROSTRUCTURES

During Treatment 6 precipitation occurred from the solution-annealed state primarily on grain boundaries. Electron diffraction of these precipitates in thin foils identified them as $M_{23}C_6$; no σ-phase was detected. The appearance of these carbides is shown on a replica in Figure 1. The grain size after Treatment 6 was 40μ. Before cold rolling during Treatment 13 the grain size was 100μ.

Precipitation occurred from the cold-worked state during Treatment 13. Favored sites for the precipitates were slip bands, deformation bands, and grain boundaries. Electron diffraction of thin foils revealed two kinds of precipitates, $M_{23}C_6$ and σ. The majority of the grain boundary precipitates are carbides but some σ is also present. The precipitates within grains on slip bands and in deformation bands are σ. Epsilon martensite is also present to some extent. The appearance of the precipitates is shown in Figure 2. Their size lies between 500 and 3000Å and they are present at a density of about 10^{13} cm^{-3}. Figure 3 shows the σ-phase particles within a grain.

Treatment 13 is similar to one used by Garofalo et al[6] to improve the creep strength of Type 316 stainless steel. These authors did not identify their fine matrix precipitates as σ. Blenkinsop and Nutting[7] have recently reported in detail on the morphology of σ-phase precipitation in a low-carbon Type 316 stainless steel. Our observations are in accord with their work.

B. TENSILE TEST RESULTS

The total elongation as a function of test temperature for samples with and without He is given in Figure 4 and all the tensile data appear in Tables 1 and 2. The strain rate was constant at 0.02 min^{-1} and the values shown in the tables are the average from two samples. Treatment 13, as expected, strengthens the alloy and reduces the ductility. The presence of He has no effect on either yield or tensile strength but does markedly reduce the ductility. Ductility loss begins above 540°C for samples given Treatment 6, but for samples given Treatment 13 loss of ductility begins above 650°C. The displacement damage from the α-particles, a possible source of hardening, appears to be annealed out at the lowest test temperature.

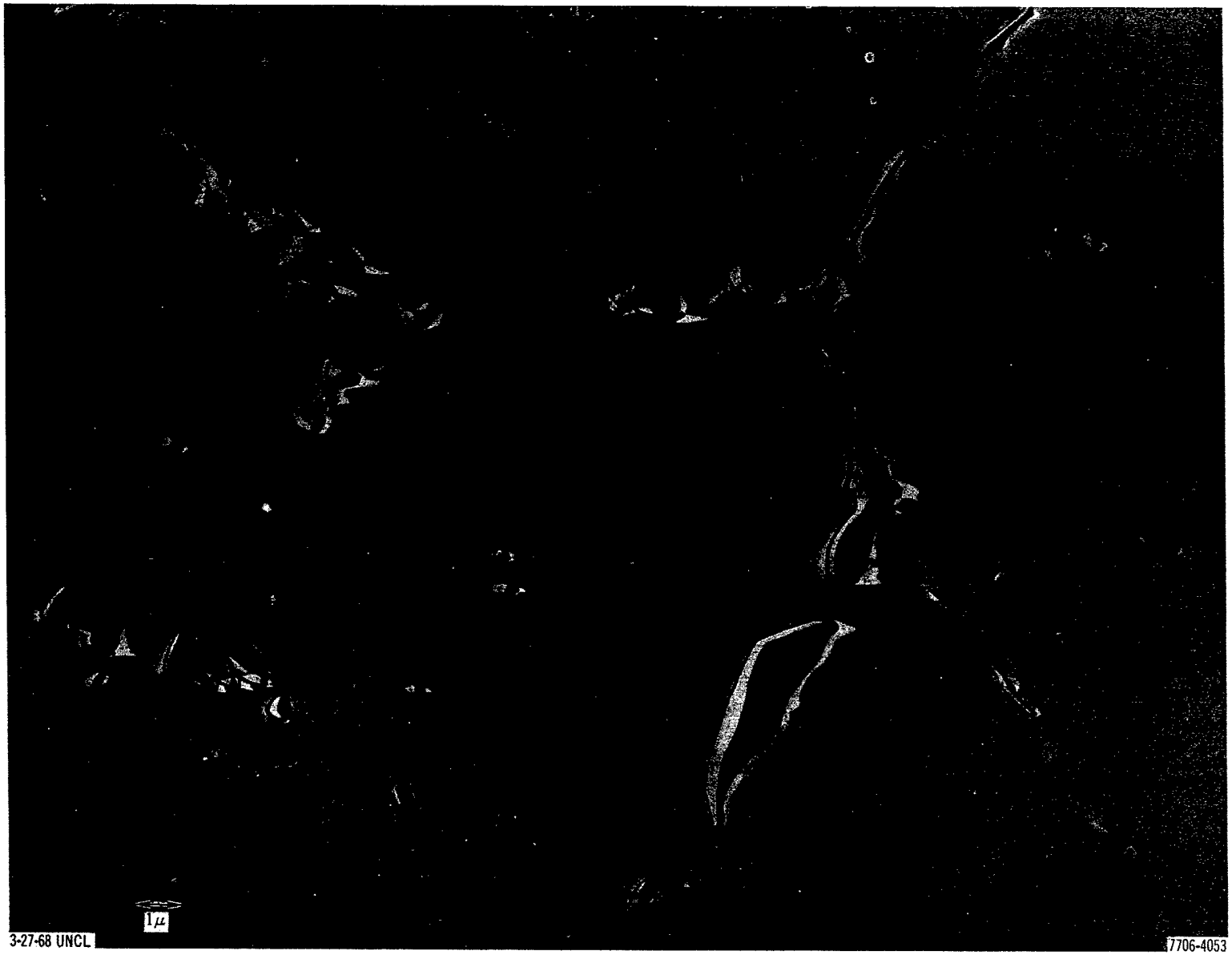

Figure 1. Replica Electron Micrograph of Type 316 Stainless Steel After Treatment 6, Showing Carbides Primarily on Grain Boundaries

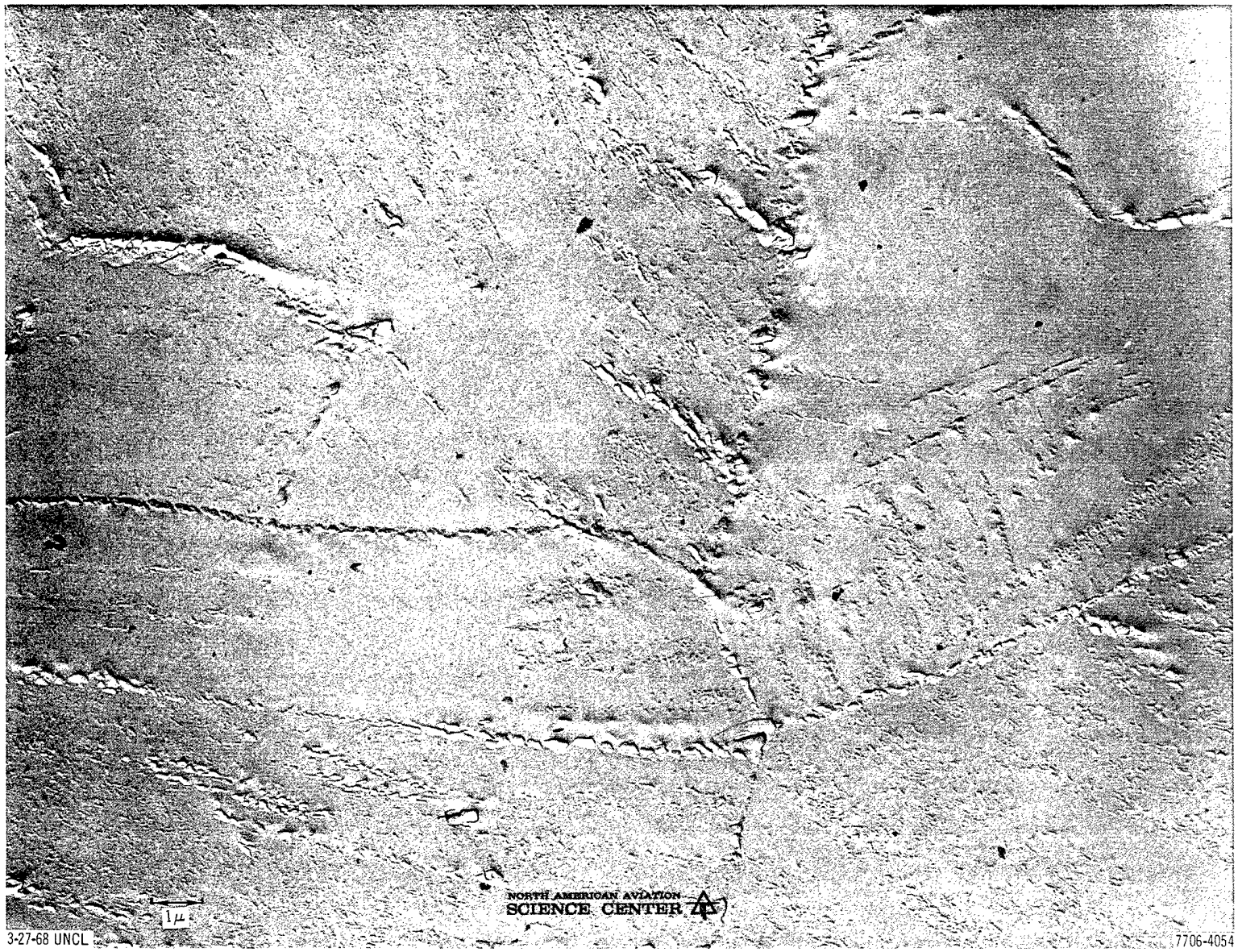

Figure 2. Replica Electron Micrograph of Type 316 Stainless Steel After Treatment 13, Showing Precipitates on Grain Boundaries and Within the Grains

Figure 3. Transmission Electron Micrograph of Type 316 Stainless Steel After Treatment 13, Showing Sigma Particles Within a Grain

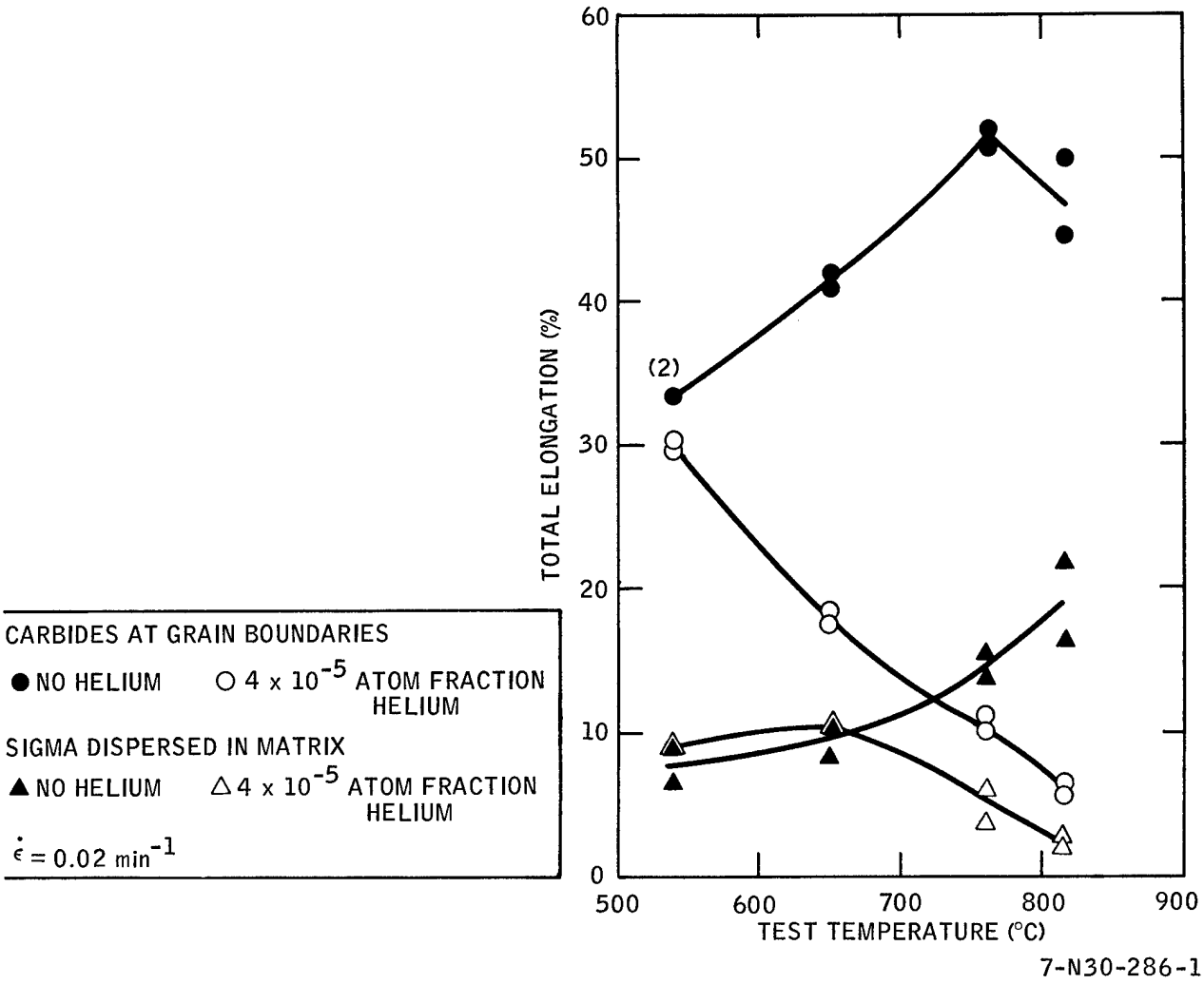

Figure 4. Total Elongation as a Function of Test Temperature for Type 316 Stainless Steel With no Helium and With 4 x 10-5 Atom Fraction Helium

TABLE 1

TENSILE TEST DATA OF TYPE 316 STAINLESS STEEL WITH TREATMENT 6

Atom Fraction Helium ($\times 10^{-5}$)	Test Temperature (°C)	Yield Strength (kpsi)	Tensile Strength (kpsi)	Elongation (%)	
				Uniform	Total
0	540	13.5	56.6	32.2	33.4
4	540	15.9	55.7	28.4	30.0
0	650	14.6	40.7	27.6	41.5
4	650	11.8	38.6	16.8	17.8
0	760	11.2	24.0	14.1	51.4
4	760	10.3	21.3	6.7	10.7
0	815	10.5	17.6	8.7	47.3
4	815	12.1	17.0	3.6	5.9

TABLE 2

TENSILE TEST DATA OF TYPE 316 STAINLESS STEEL WITH TREATMENT 13

Atom Fraction Helium ($\times 10^{-5}$)	Test Temperature (°C)	Yield Strength (kpsi)	Tensile Strength (kpsi)	Elongation (%)	
				Uniform	Total
0	540	19.1	68.2	7.0	7.8
4 (one sample)	540	13.3	68.3	8.0	9.1
0	650	13.8	55.1	5.1	9.5
4	650	14.0	52.7	5.0	10.8
0	760	13.9	36.6	1.6	14.7
4	760	17.0	34.9	1.4	5.0
0	815	14.4	26.0	1.4	19.2
4	815	12.8	26.6	1.4	2.7

C. METALLOGRAPHY OF TESTED SAMPLES

At 540°C all samples given either treatment with or without He failed transgranularly. The mechanism of shear-rupture was operating as evidenced by the shear-rupture dimples in Figure 5 which typifies all fractographs of samples tested at this temperature. The mode of failure of samples given Treatment 13 with or without He, and of samples given Treatment 6 without He was transgranular at 650°C. However, samples given Treatment 6 with He showed a mixture of transgranular and intergranular failure.

At 760°C all samples with He failed intergranularly. Of the samples without, those given Treatment 6 still failed transgranularly, whereas those given Treatment 13 had a mixed failure. Intergranular cracks were readily detectable in helium-containing samples, especially in those given Treatment 13, but were relatively rare in samples without He. Figure 6 shows such cracks.

Replicas for electron microscopy were taken of tested samples on a plane parallel to the tensile axis and to the broad surface of the samples. By this method incipient cracks or voids as small as 3000Å can be detected. These negative replicas reveal a depression on the sample surface by the presence of a light shadow adjacent to a dark area.

Figure 7 shows voids in samples with He tested at 760°C. They are situated on grain boundaries adjacent to carbide particles. The tensile axis is parallel to the direction of the white shadow. The relative frequency of these voids parallels that of grain-boundary cracks as stated above. The great majority of voids were associated with grain-boundary carbide particles, and even those which appear isolated on a grain boundary may be next to a carbide particle in another plane.

Helium bubbles were found in samples given either treatment after testing at 760°C (bubbles were not detected after tests at 540 and 650°C) and were generally located on grain boundaries, dislocations, and precipitates. Figure 8 shows He bubbles in samples given Treatment 6. The average bubble size is less than 100Å although some bubbles 1000Å and greater are present on grain boundaries and attached to carbide particles (see Figure 8c).

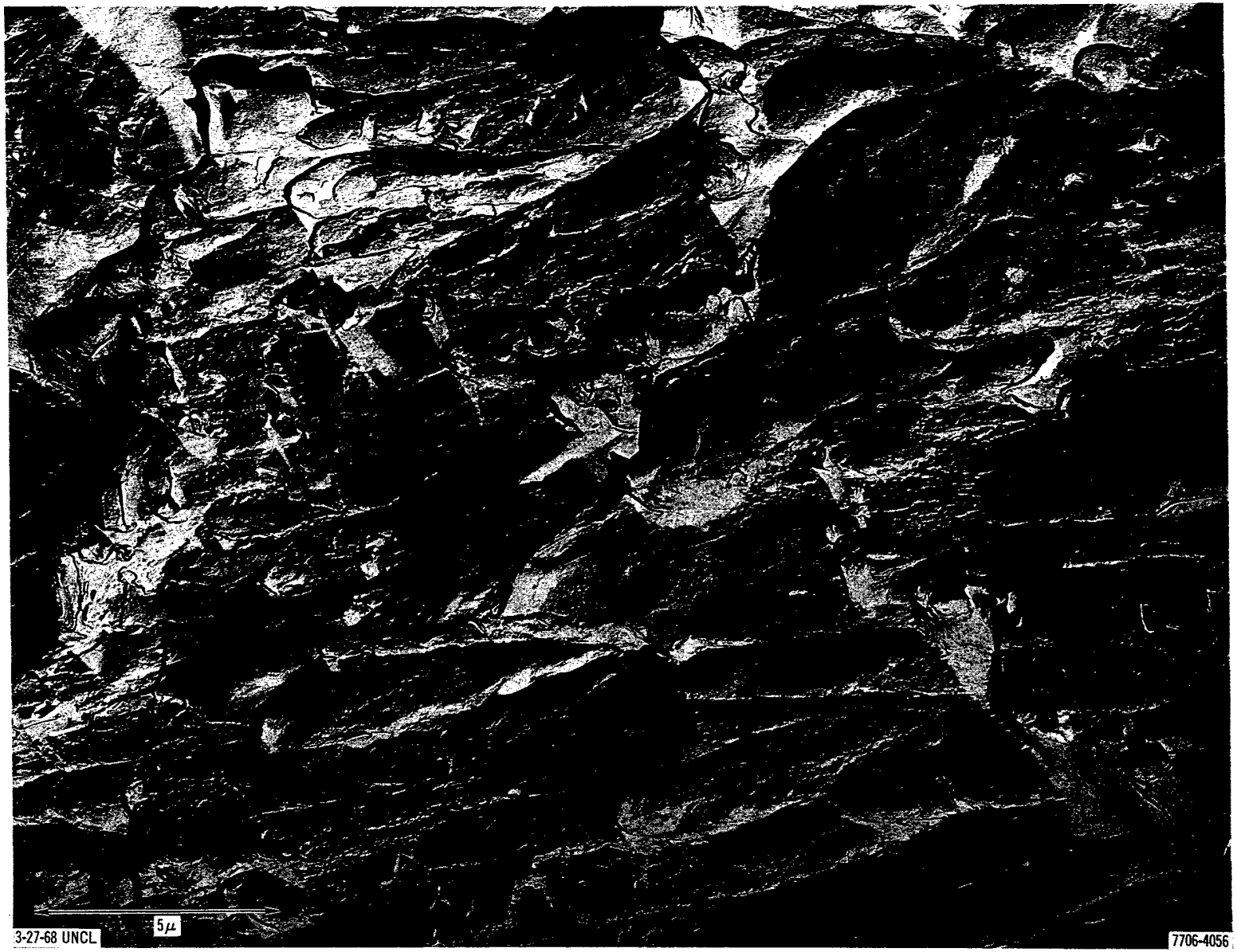

Figure 5. Fractograph of Type 316 Stainless Steel Without Helium Tested at 540°C, Showing Shear-Rupture Dimples

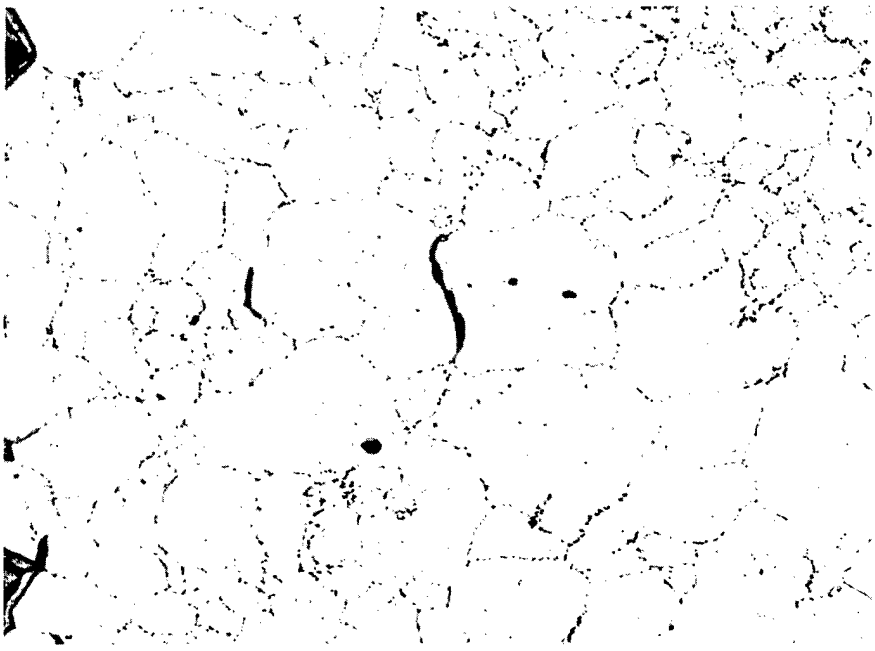

a. With Treatment 6

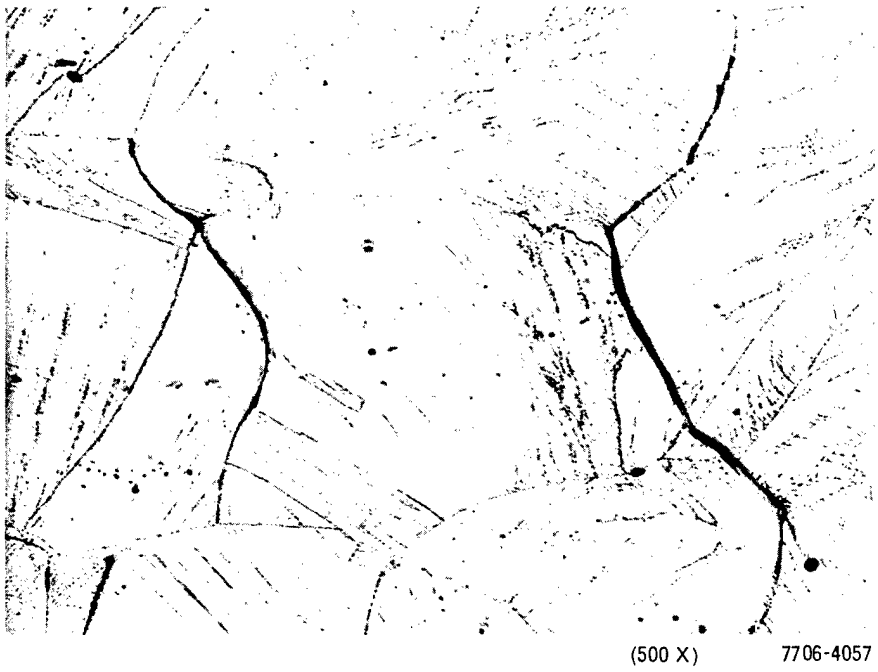

b. With Treatment 13

Figure 6. Light Micrographs of Type 316 Stainless Steel With 4×10^{-5} Atom Fraction Helium Tested at 760°C, Showing Intergranular Cracks

Figure 7a. Replica Electron Micrograph of Type 316 Stainless Steel With 4 x 10^{-5} Atom Fraction Helium Tested at 760°C, Showing Voids Adjacent to Grain-Boundary Carbides, Treatment 6

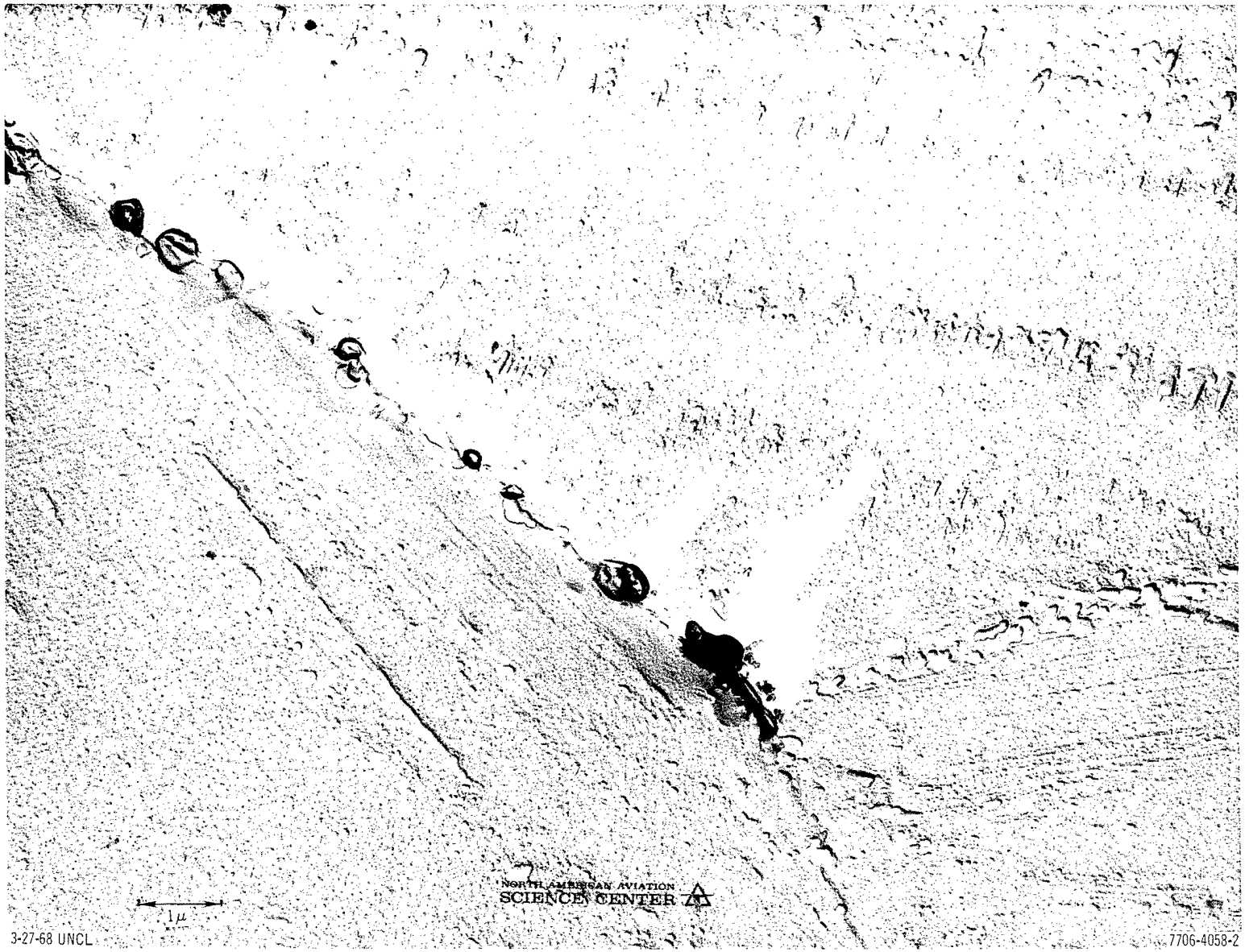

Figure 7b. Replica Electron Micrograph of Type 316 Stainless Steel With 4 x 10-5 Atom Fraction Helium Tested at 760°C, Showing Voids Adjacent to Grain-Boundary Carbides, Treatment 13

Figure 8a. Transmission Electron Micrograph Showing Helium Bubbles in Type 316 Stainless Steel Given Treatment 6 With 4×10^{-5} Atom Fraction Helium Tested at 760°C

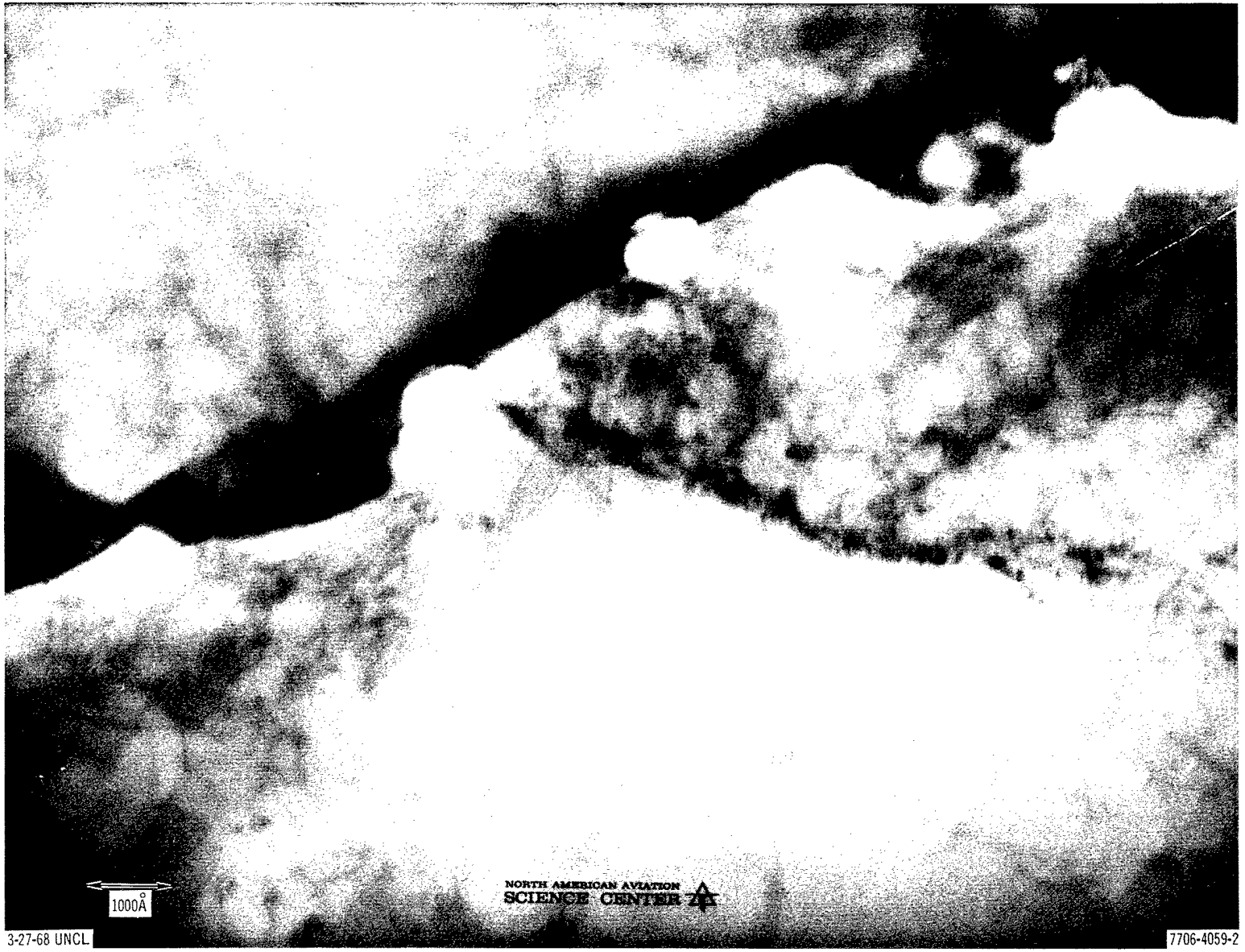

Figure 8b. Transmission Electron Micrograph Showing Helium Bubbles in Type 316 Stainless Steel Given Treatment 6 With 4×10^{-5} Atom Fraction Helium Tested at 760°C

Figure 8c. Transmission Electron Micrograph Showing Helium Bubbles in Type 316 Stainless Steel Given Treatment 6 With 4×10^{-5} Atom Fraction Helium Tested at 760°C

Figure 9 shows He bubbles in samples given Treatment 13. Their average size is also less than 100Å but a very large bubble (>2000Å in one dimension) has formed on a grain boundary (see Figure 9b). Most of the small bubbles are attached to σ-particles. Large bubbles were significantly less prevalent in samples of Treatment 13 than in 6.

Fractured carbide particles were found in samples given Treatment 6, with or without helium, after testing at all temperatures (except 815°C, for which no metallography was done). No fractured carbides were found in samples given Treatment 13. Figure 10 shows several examples of fractured carbides on grain boundaries and also decohesion or separation at the carbide-matrix interface. The cracks formed in the carbides were not observed to grow into the adjacent grain.

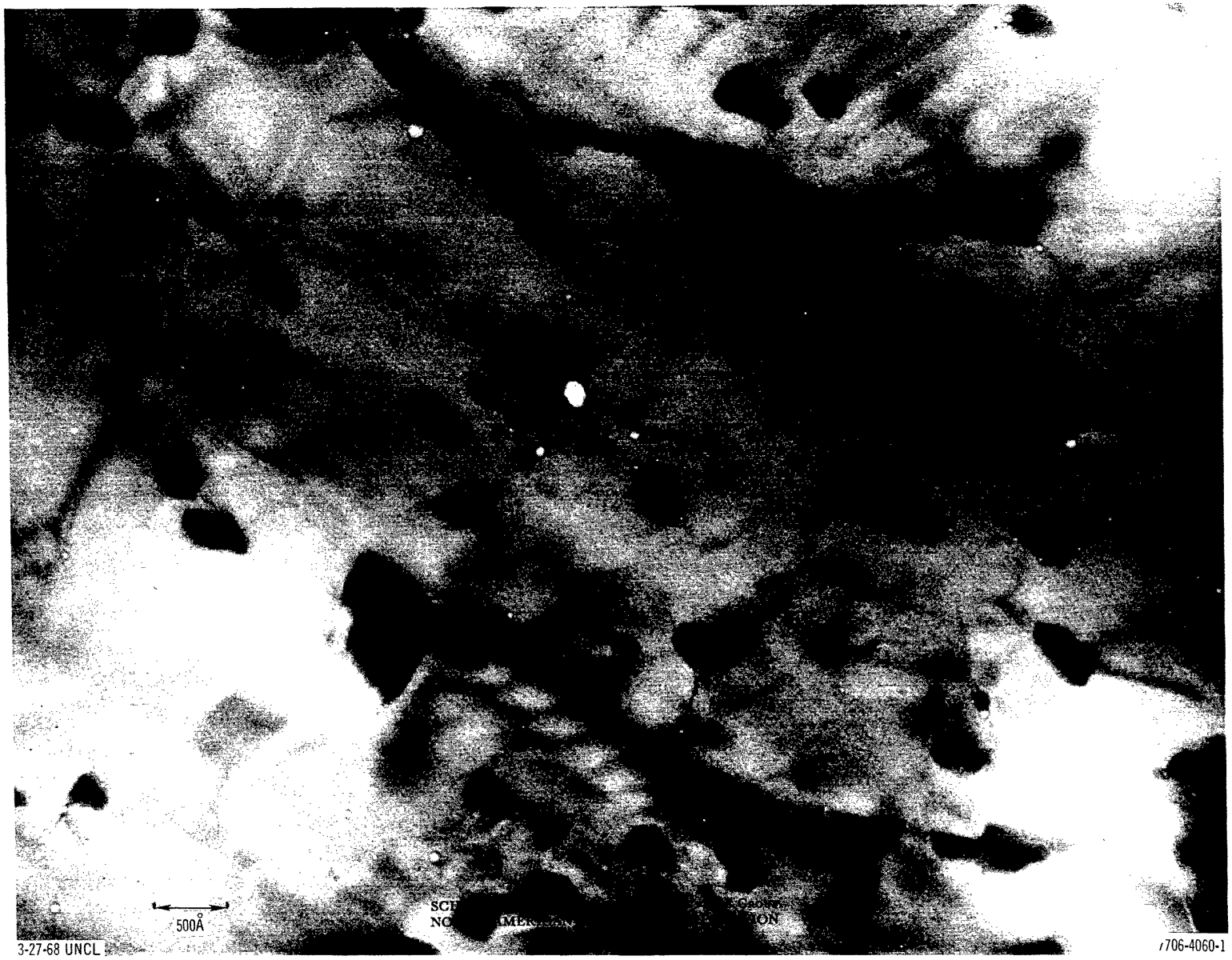

Figure 9a. Transmission Electron Micrograph Showing Helium Bubbles in Type 316 Stainless Steel Given Treatment 13 With 4 x 10^{-5} Atom Fraction Helium Tested at 760°C

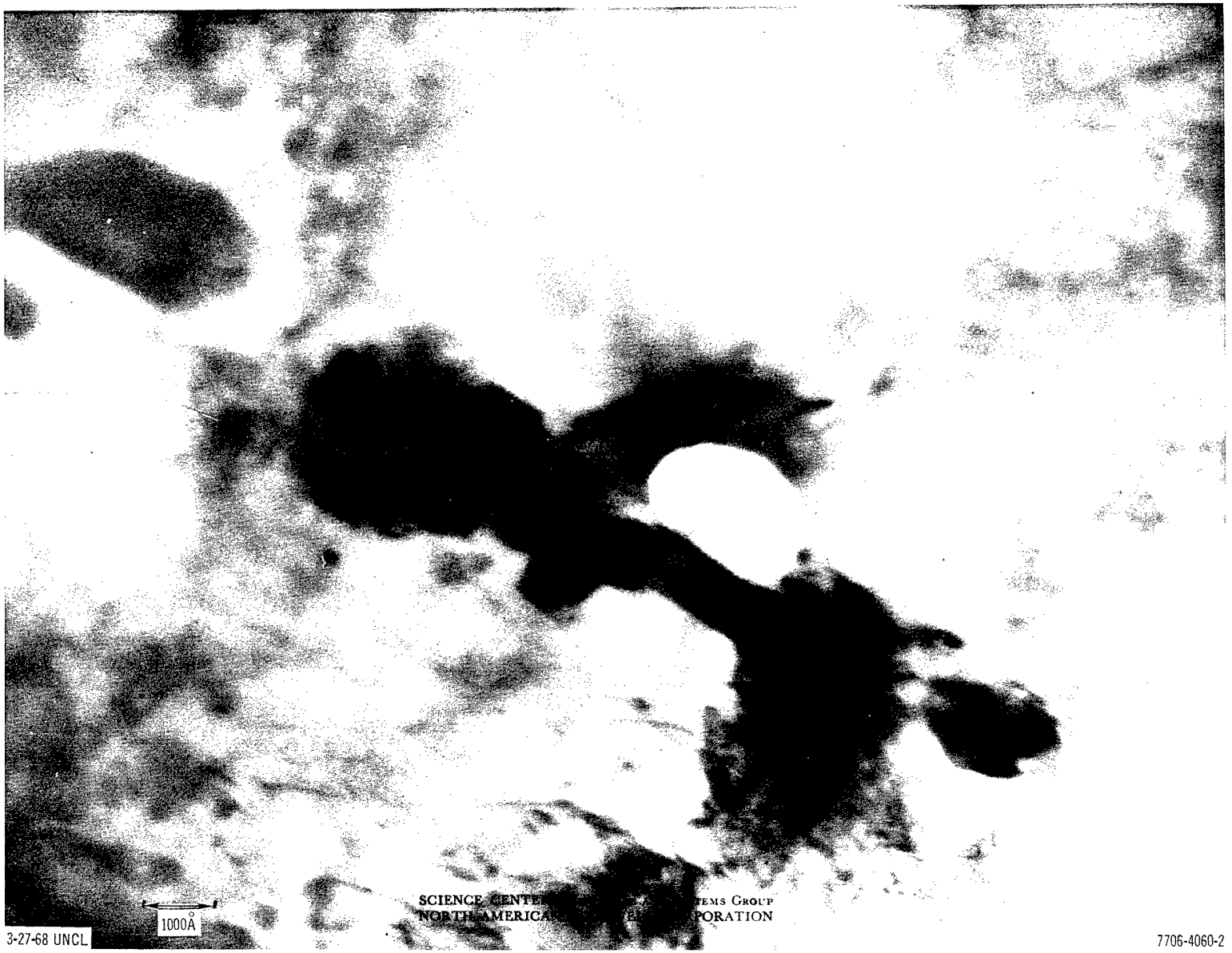

Figure 9b. Transmission Electron Micrograph Showing Helium Bubbles in Type 316 Stainless Steel Given Treatment 13 with 4×10^{-5} Atom Fraction Helium Tested at 760°C

Figure 10a. Transmission Electron Micrograph Showing Fractured Carbide Particles in Type 316 Stainless Steel Given Treatment 6 With 4×10^{-5} Atom Fraction Helium, Tested at 540°C

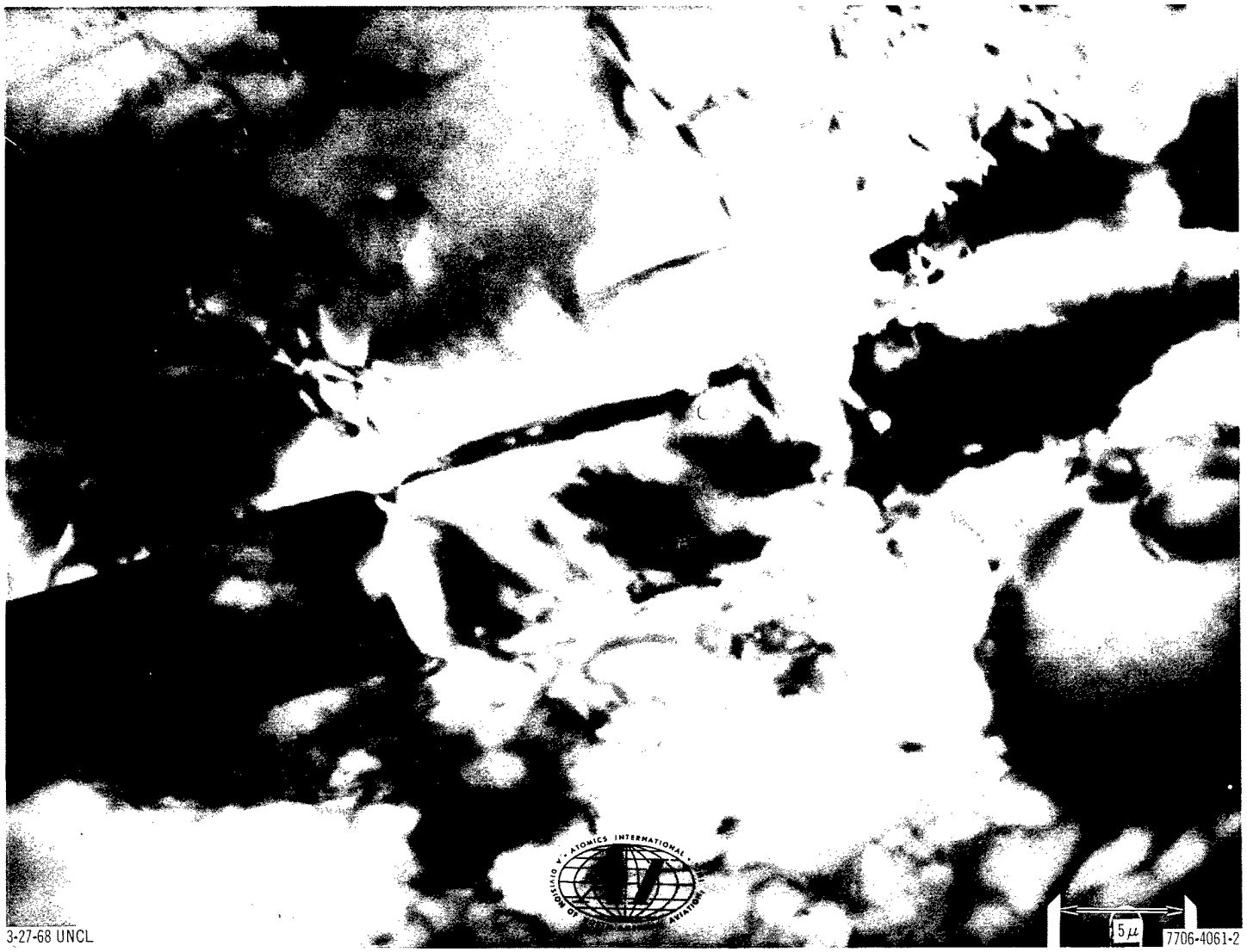

Figure 10b. Transmission Electron Micrograph Showing Fractured Carbide Particles in Type 316 Stainless Steel Given Treatment 6 With 4×10^{-5} Atom Fraction Helium, Tested at 650°C

IV. DISCUSSION

Loss of ductility due to helium is always accompanied by a failure that is partially or completely intergranular and by the presence of intergranular cracks along the gauge length. These cracks in their incipient state are located adjacent to grain-boundary carbide particles (Figure 7). Grain-boundary sliding, which probably occurs during testing, is obstructed by the presence of these carbide particles. In this situation voids are nucleated at the particle-matrix interface, and the mechanism has been described for a variety of alloys.[8-10]

This mechanism is valid whether or not He is present; when it is, grain-boundary voids and cracks are present to a much greater extent for equivalent amounts of strain. The stress necessary to nucleate a void at an obstacle on the grain boundary was estimated to be[11]

$$\sigma_s = \left(\frac{12\mu\gamma_s}{\pi L}\right) ,$$

where μ is the shear modulus, γ_s is the interphase surface energy, and L is the length of sliding boundary between obstacles. A He bubble on a grain-boundary carbide could effectively reduce σ_s to zero since a He bubble is truly a void already and no nucleation is necessary. Growth of the void to a crack will occur by further sliding and through the action of a stress normal to the boundary. Figures 8b, 8c, and 9b are examples of bubbles on grain-boundary carbides which have the potential of growing into cracks. This mechanism of He embrittlement was also concluded to operate in the case of Type 304 stainless steel.[5]

Another factor responsible for intergranular crack initiation at carbide particles (in the absence of He bubbles) is the probable low value of γ_s. This allows separation of the carbide-matrix interface at low values of σ_s. It is also likely that cracked carbide particles are another source of grain-boundary cracks. Decohesion at the carbide-matrix interface and cracked carbides are more important in the mechanisms of failure when He is absent. At low temperatures, Barnby[12] has shown how cracked carbides start a transgranular failure.

Samples given Treatment 13 show loss of ductility beginning above 650°C, while at this temperature those given Treatment 6 have already lost more than half their ductility. This is due to the effectiveness of the high density of σ-particles (10^{13} cm^{-3}) in trapping He (seen in Figure 9a as bubbles attached to the particles), thereby delaying the accumulation of He at grain boundaries.

It is unlikely that trapped He bubbles leave the particles at higher temperatures and migrate to the boundary. Rather, untrapped He eventually arrives, as atoms or very small bubbles, at the boundary to yield a concentration high enough to form large bubbles on carbide particles.

V. CONCLUSIONS

The following conclusions can be drawn from this study:

1. Cyclotron injection of helium into tensile samples of Type 316 stainless steel at concentrations of 4×10^{-5} atom fraction results in ductility loss at test temperatures above 540 and 650°C for samples given a precipitation anneal from the solution-annealed or cold-rolled condition, respectively.

2. Loss of ductility, as measured by elongation at failure, is associated with premature intergranular cracking which originates at grain-boundary carbide particles, presumably through the action of grain-boundary sliding.

3. Helium aids grain-boundary cracking by forming bubbles on carbide particles, thus greatly reducing the amount of grain-boundary sliding needed to form a void.

4. A fine dispersion of precipitates is effective in trapping helium bubbles, thereby raising the temperature at which ductility loss appears.

REFERENCES

1. G. H. Broomfield, D. R. Harries, and A. C. Roberts, JISI, 1965, 203, 502-6
2. R. S. Barnes, Nature, 1965, 206, 1307-10
3. A. F. Rowcliffe, J. Nuc. Mat., 1966, 18, 60-65
4. H. Alter and C. E. Weber, J. Nuc. Mat., 1965, 16, 68-73
5. D. Kramer, H. R. Brager, C. G. Rhodes, and A. G. Pard, NAA-SR-12601 (also in J. Nuc. Mat., 1968, 25) (121-131)
6. F. Garofalo, F. von Gemingen, and W. F. Domis, Trans.ASM, 1961, 54, 430-44
7. P. A. Blenkinsop and J. Nutting, JISI, 1967, 205, 953-958
8. J. R. Low, "Fracture of Solids," 197-236, 1963, Gordon and Breach
9. J. D. Meakin and N. J. Petch, Ibid, 393-415
10. J. E. Harris, Trans. Met. Soc. AIME, 1965, 233, 1509-16
11. C. W. Weaver, Acta Met., 1960, 8, 343-44
12. J. T. Barnby, Acta Met., 1967, 15, 903-9